



Effect of the preparation method in the size of chitosan nanoparticles for the removal of allura red dye

Yedidia Villegas-Peralta¹ · Ma. A. Correa-Murrieta¹ · Edna R. Meza-Escalante¹ · Eric Flores-Aquino² · Jesús Álvarez-Sánchez¹ · Reyna G. Sánchez-Duarte¹

Received: 17 July 2018 / Revised: 30 October 2018 / Accepted: 8 November 2018 /

Published online: 14 November 2018

© Springer-Verlag GmbH Germany, part of Springer Nature 2018

Abstract

Nanoparticles of chitosan–tripolyphosphate through two ionic gelation methods (Np1 and Np2) with different dosages of TPP and stirring time were prepared and characterized (FTIR, TEM, SEM–EDS, AFM, XRD, DLS and BET) for the removal of an allura red dye. Np1 and Np2 were obtained with a diameter size of 315.5 nm and 437.4 nm, respectively, both with low polydispersity. The influence on smaller particle size was defined by a low concentration of chitosan solution (0.2 mg/mL) and a higher dosage of TPP (1 mg/mL), while the stirring time did not affect the particle size. Dye removal was placed in batch mode by varying adsorbent dosage, time and pH. The removal percentage (R%) in Np1 decreased with an increase in adsorbent dosage at pH 4 and 6, while Np2 remained constant at pH 2, 4 and 6. Adsorption essays in Np1 and Np2 revealed that under pH 2, an adsorbent dosage of 0.01 g and a contact time of 5 min, the adsorptions are complete. Np2 was recognized as the best adsorbent in comparison with Np1 due to the highest R% under several pHs. This research has demonstrated that the obtained nanoparticles by ionic gelation are suitable for removal of azo dyes in water.

Keywords Adsorption · Azo dyes · Ionic gelation · Chitosan nanoparticles · Removal

✉ Reyna G. Sánchez-Duarte
reyna.sanchez@itson.edu.mx

¹ Departamento de Ciencias del Agua y Medio Ambiente, Instituto Tecnológico de Sonora, 5 de Febrero 818 Sur, 85000 Ciudad Obregón, Sonora, Mexico

² Laboratorio de Nanocatálisis, Centro de Nanociencias y Nanotecnología, Universidad Autónoma de México, Km 107 Carretera Tijuana-Ensenada, 22860 Ensenada, BC, México

Introduction

Facing a concerning situation of the pollution of natural resources, especially water, there has been a growing interest in solving these problems through low-cost solutions. Owing to the presence of polysaccharides in nature, new alternatives for water remediation have been explored and developed. One of the natural polysaccharides used in this area is chitin. Chitin, poly (β -(1 \rightarrow 4)-*N*-acetyl-D-glucosamine), is the most important polysaccharide; this biopolymer is synthesized by a great number of living organisms; it is the most abundant polymer after cellulose [1]. On the other side, chitosan is a natural cationic polysaccharide obtained through the *N*-deacetylation of chitin, a product found in the shell of crustaceans [2]. Chitosan has been studied for its excellent biocompatibility, biodegradability, cationic character and null toxicity [3]. Furthermore, it has reactive groups such as hydroxyls and amino groups along its chain, which grants its properties of being nontoxic and biologically degradable and also increases its potential for synthesis [4].

Due to those characteristics, the formation of hydrogels, membranes, microparticles and nanoparticles is possible and makes it a material of interest to adsorb water pollutants. Nevertheless, the use of this polysaccharide has been limited due to its original form. In order to improve chitosan properties, it has been used as cross-linking chemical agents. Sodium tripolyphosphate is the most commonly used cross-linker for ionic gelation due to its negative charges [5] and has been successfully used to obtain nanoparticles and microparticles of chitosan.

Among the described techniques for the preparation of nanoparticles and the use of sodium tripolyphosphate as a cross-linking agent, emulsion cross-linking and ionic gelation methods [6] are the most used, because its processes are easy to control, and do not use large amount of organic solvents and high temperatures [7].

Chitosan in combination with sodium tripolyphosphate offers a great potential to be developed in a diversity of areas. Various types of adsorbents in a nanoparticle complex are used to remove dyes from water and are being investigated; one of them are the MgO nanoparticles used to remove Reactive Blue 19 and Reactive Red 198 reported by Moussavi and Mahmoudi [8]. Also, Lipatova et al. [9] used chitosan nanoparticles immobilized in activated PET fiber to remove anionic dyes: Direct Blue-86 and Reactive Blue 21. Another are the nanofibrous membranes of pure chitosan that has been used to remove Acid Blue-113 and reported by Li et al. [10]. El-Harby et al. [11] demonstrated that terephthaloyl thiourea cross-linked chitosan hydrogels are able to adsorb Congo red dye in an aqueous solution.

There is information about the preparation of chitosan–sodium tripolyphosphate nanoparticles, but mainly used in biomedical applications. For this reason, the aim of this work is to synthesize cross-linking chitosan–sodium tripolyphosphate nanoparticles using ionic gelation method with variation in the dosage of TPP and stirring time, as well as the comparison between their physicochemical characterizations for allura red dye removal in aqueous solutions.

Materials and methods

Materials

Sodium tripolyphosphate ($\text{Na}_5\text{P}_3\text{O}_{10}$, reagent grade, 85%) and sodium hydroxide (NaOH, reagent grade, 97%) were purchased from Sigma-Aldrich (St. Louis, MO, USA). Glacial acetic acid (CH_3COOH , reagent grade, 99.5%) was purchased from Fermont (Monterrey, México). Chitin was isolated from shrimp shells. Chitosan was 92.16% of deacetylation degree (DD) and was 3.16×10^5 g/mol of molecular weight. Allura Red dye (CAS Number 25956-17-6, reagent grade, 80%) purchased from Sigma-Aldrich.

Nanoparticles preparation by ionic gelation method 1

Ionic gelation nanoparticles method 1 was obtained using ionic gelation procedure by Calvo [12], with modifications. A 0.2% (w/v) chitosan solution in 5% (v/v) acid acetic was prepared and left to stand for 24 h, and then, the solution was filtered. Later, a solution of 1% (w/v) TPP was dripped under continuous stirring for 36 h at 100 rpm (Fig. 1 Np1). Suspension was centrifuged for 1 h at 6000 rpm. Finally, the precipitation was lyophilized by freeze-drying (LabConco FreeZone 1).

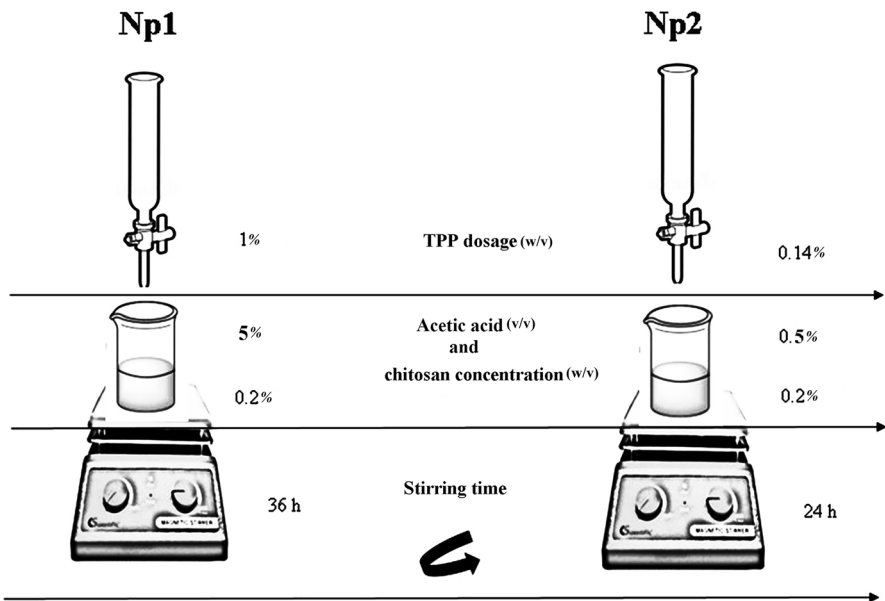


Fig. 1 Main differences in the formation of Np1 and Np2 by the gelation process

Nanoparticles preparation by ionic gelation method 2

To obtain the nanoparticles by ionic gelation method 2 (Np2), the method proposed by Hu et al. [13] was used and begins as follows: a solution of 0.2% (w/v) chitosan was prepared in 0.5% (v/v) acetic solution leaving rest for 24 h. After this period, the solution was filtered. Later, the solution was kept under stirring for 20 min, while a solution of 0.14% (w/v) TPP was added (Fig. 1 Np2). After, it was frozen for 24 h and was subsequently defrosted. This emulsion was stirred by 24 h and lastly centrifuged at 6000 rpm for 40 min. The supernatant was retired, and the residual solution was washed with distilled water. The same procedure was carried out twice for 20 min. At the end, the emulsion was lyophilized in order to be characterized.

Np1 and Np2 characterization

Functional groups of the cross-linking nanoparticles were taken with Fourier transform infrared spectroscopy (FTIR) on a Thermo Scientific Spectrum model Nicolet iS5. Samples were prepared in a KBr pellet in a relation of weight of 0.02:0.45 (sample: KBr). The range of the analysis was from 4000 to 400 cm^{-1} region with a resolution of 4 cm^{-1} . Previously, the samples were dried at 110 °C for 1 h. An accessory of transmission iD1 was used to collect the sample. The OMNIC software was used to make the correction for KBr. At this stage, the activated sites after the cross-linking were determined, and a comparison between pure chitosan, Np1 and Np2 was analyzed.

The surface characteristics of the samples were collected using a scanning electron microscope (SEM, JEOL JSM-5300) with a detector to perform chemical analysis by means of energy dispersion (EDS) operated at 10 kV; the samples were placed on a carbon base. The present elements were determined for each sample. The specific surface area was determined by BET (Brunauer–Emmett–Teller) using the nitrogen adsorption method (Quantachrome Autosorb-iQ-C, USA). The sample was dried under 40 °C for 12 h as a pretreatment.

Surface topography and surface roughness were analyzed by atomic force microscopy (AFM, Workshop TM). The range of measurement was 50 μm taken at ambient conditions. All the samples were prepared from a 10% (w/v) nanoparticle solution in 100 mL of 10% (v/v) acetic acid. A drop of each sample was placed on the surface of polyacrylic and then on a steel coin. Samples were dried at room temperature. The cantilever (material) was the same for all the measurements with the values of drive amplitude set in the range 800–1200 mV. Captured images were treated using the software Gwyddion.

The crystallinity was recorded using an X-ray diffractometer Philips X'pert MPD (XRD) radiation at 40 kV and 45 mA in the 2θ range of 5–60°.

To define the size of the particles, the samples were measured with transmission electron microscopy (TEM, JEOL JEM-2010), which was operated at 200 kV. The sample was suspended in isopropyl alcohol and then was sonicated for 10 min and placed in a cooper grid (Lacey carbon, SPI supplies) to be analyzed. The technique

of dynamic light dispersion (DLS) was used to determine the hydrodynamic diameter and the size distribution (PDI) by using an equipment Nano Zetasizer, Malvern Instruments at 633 nm wavelength.

Adsorption essays of allura red dye

The nanoparticles were studied to determine the adsorption capacity of allura red dye expressed in removal percentage (R%). Experiments were carried out in batch mode, using an adsorbent dry mass from 0.01 to 0.05 g in a volume of 50 mL of dye solution at 25 ppm, under mechanical stirring at pH 2, 4 and 6. After a contact time of 15 min, dye solutions were separated using a centrifuge (VWR Clinical 200) at 6000 rpm for 30 min.

The initial and final concentrations of RA dye were obtained from the information of the wavelength at 510 nm using a visible spectrophotometer (Thermo Spectronic Genesys 20 (4001/4)). The data collected from the tests were used to calculate the dye removal using Eq. 1.

$$R(\%) = \frac{C_i - C_f}{C_i} \times 100 \quad (1)$$

where R(%) denoted the percentage of dye removal (%); C_i and C_f are the initial and final concentrations of dye (mg/mL).

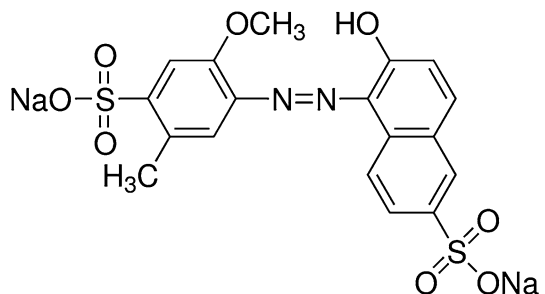
For a better comprehension of the behavior of AR dye removal, the effect of contact time was assessed by considering the optimal mass of adsorbent resulted from previous essays. Experiments were carried out at an interval time from 5 to 25 min. The Fig. 2 shows the structural formula of the allura red dye used in the essay of adsorption.

Results and discussion

Characterization of cross-linking nanoparticles

In this part of the study, the determination of activated functional groups after the cross-linking was analyzed. TPP was used to prepare chitosan nanoparticles because

Fig. 2 Structural formula of allura red dye



it is nontoxic and multivalent [6]. TPP is well known because it has a negatively charged particle due to phosphate radical (PO_4^-), and it makes an ionic interaction with the amino groups of the chitosan which is charged positively via electrostatic attraction.

Functional groups

The infrared spectrum (IR) of CS, Np1 and Np2 is shown in Fig. 3.

The IR spectrum of shrimp chitosan (Fig. 3a) was found to be similar to the commercial chitosan reported by Sini et al. [14]. The FTIR absorbance band at 3450.31 cm^{-1} of chitosan revealed O–H stretching, and in the same region the presence of N–H stretching, both groups are presented in the molecular structure of chitosan, and it was consistent to the reported by Kong [15] and De Andrade et al. [16]. The absorbance at 1651.9 cm^{-1} , was identified as the amide I, this was appreciated as a peak with low intensity. Literature by Dimzon et al. [17] showed the amide I and amide II absorption bands at 1630 cm^{-1} and 1660 cm^{-1} , respectively. A similar result was found in this paper with a peak in 1619 cm^{-1} and 1651.9 cm^{-1} . Brugnertotto et al. [18] quote the absorbance ranges between 1655 cm^{-1} and 1625 cm^{-1} for amide I, which also agree with the result in this work. The band at 2926.04 cm^{-1} in this research corroborated the –CH stretching. The band at 1324.54 cm^{-1} as an indicator of the presence of –OH, –NH₂, –CO groups was considered and was used

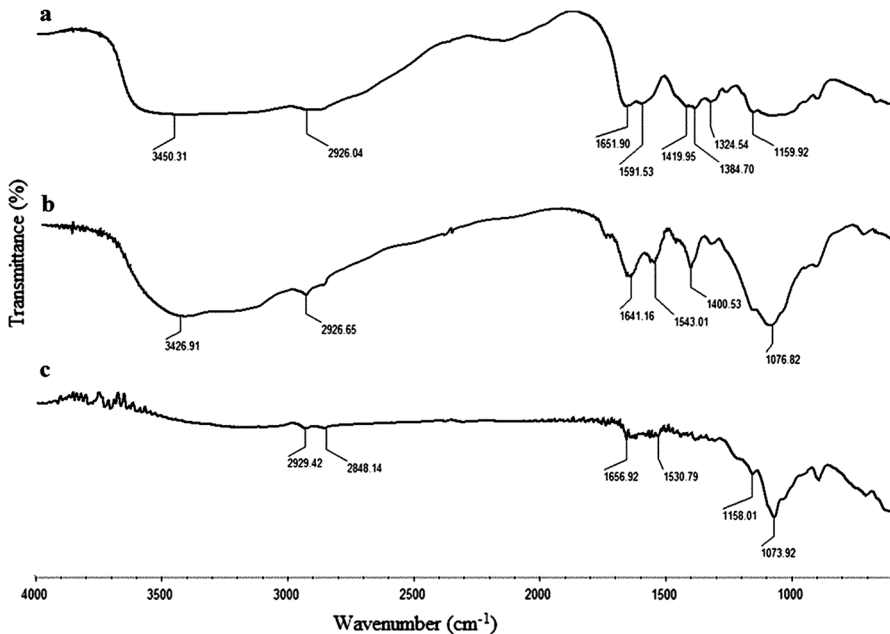


Fig. 3 Infrared spectrum of **a** raw chitosan, **b** nanoparticles by ionic gelation method 1 (Np1) and **c** nanoparticles by ionic gelation method 2 (Np2)

as a reference band to define deacetylation degree. The -NH (primary and secondary) was identified within the range between 1324.54 cm^{-1} and 1384.70 cm^{-1} . The peak at 1419.95 cm^{-1} was considered as the band referred at 1420 cm^{-1} (CH of CH_2 bending) with a very small intensity. The transmittance value of 1159.92 cm^{-1} showed the bridge -COC stretching (polysaccharide) result which is consistent with the literature reported by Blanquicet et al. [19], Lin and Lin [20], and Sun and Wang [21]. The above information made possible calculate the deacetylation degree of chitosan and verify the presence of amino groups in the chitosan chain, resulting in 92.16%.

The Np1 infrared spectrum (Fig. 3b) presented a curve in the range of $3700\text{--}3500\text{ cm}^{-1}$ that was represented by OH stretching followed by NH stretching, and it is very similar to pure chitosan (Fig. 3a). The peak found at 3426.91 cm^{-1} was represented by OH stretching. The peak at 2926.65 cm^{-1} corresponds to -CH stretching. It is important to observe the reduction of the peak corresponding to amide I at 1641.16 cm^{-1} and the disappearance of the peak of amide II that was displaced to 1543.01 cm^{-1} , which indicates a cross-linking of the amino groups, and suggests an interaction between the TPP and chitosan. This behavior is also evidenced by the decrease in the degree of deacetylation of the nanoparticles made under the ionic gelation method 1 (81.21%) and method 2 (80%) compared to raw chitosan.

An interesting characteristic of the TPP interaction is the intensification and the slight displacement of characteristic bands of functional groups -NH and -COC , at 1400.53 cm^{-1} and 1153.56 cm^{-1} , respectively. The band at 1076.82 cm^{-1} showed a high intensity that means an interaction of amino groups, and this behavior is assigned to P=O groups of TPP.

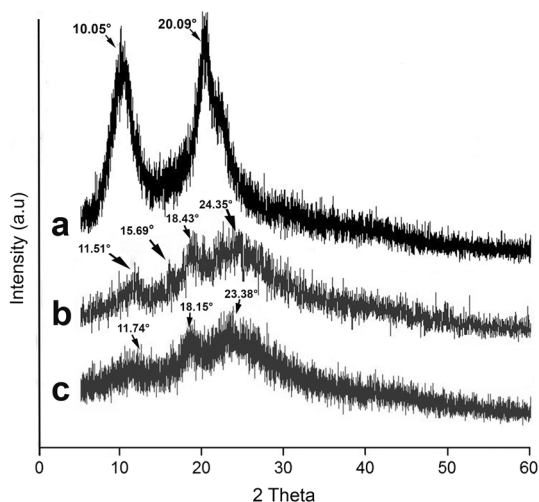
In the Np2 infrared spectrum (Fig. 3c), the weak formation of the peaks at 1656.92 cm^{-1} and 1530.79 cm^{-1} was identified as amide I and amide II. The band at 1073.92 cm^{-1} is a peak that cannot be left unnoticed, due to its high intensity, leading to affirm the correct process to cross-linked particles using TPP, and the same behavior was presented with the process of method 1. The interference observed in the range of $3800\text{--}3600\text{ cm}^{-1}$ at the beginning of the curve suggested no well-dried sample, but this does not affect the result after the 3500 cm^{-1} band. The bond C-O is illustrated in the absorbance at 1158.01 cm^{-1} , corresponding to C-O-C groups, which is the same case reported by Nosal et al. [22].

The peaks at 2926.04 cm^{-1} , 2926.65 cm^{-1} and 2929.42 cm^{-1} on all spectrums in Fig. 3 were attributed to vibrations of carbon dioxide; data are shared by Brugnerotto et al. [18]. The information obtained from each spectrum confirmed the TPP/chitosan cross-linking.

Crystallinity

The XRD diffraction of CS (a), Np2 (b) and Np1 (c) is observed in Fig. 4. The diffractions of Np1 and Np2 showed significant differences on the crystallinity profile compared to raw chitosan. In Fig. 4, the XRD profile of raw chitosan (a) showed its natural semi-crystal structure on the peaks at $2\theta=20.09^\circ$ and 10.05° , and they were

Fig. 4 XRD patterns profile for **a** raw chitosan, **b** Np2 and **c** Np1



attributed to the crystalline region formed by the hydrogen bond among the amino groups in the chitosan chain; the same data are reported by Martins et al. [23] and Walke et al. [24].

The diffraction patterns of Np1 (c) and Np2 (b) in Fig. 4 presented a chitosan chain reorganization with peaks at $2\theta = 11.77^\circ$, 15.69° , 18.43° and 24.35° for Np2 and $2\theta = 11.74^\circ$, 18.15° and 23.38° for Np1; both methods showed similar peaks attributed to the appearance of the phosphates belonging to the molecule of TPP. Comparing the crystallinity between Np2 and Np1, they are lower than chitosan as a result of TPP concentration, which provides rigidity to the chain. During the interaction of phosphate groups of TPP and amino groups of chitosan, there occurs a loss in the compaction of the inter- and intra-chain bonding of the molecule, which is manifested by a decrease in crystallinity. Similar reduction in crystallinity peaks was reported by Deshpande et al. [25]. In this way, Np2 presented a higher crystallinity compared to Np1, which is related to TEM results, and attributed to the used small dosage of TPP. The majority of the nanoparticles (b and c) were amorphous and do not present well-defined crystalline arrangement.

Surface roughness

The image with two- and three-dimensional surface topography of Np1 and Np2 is shown in Fig. 5a–d. The image was taken using a resolution of $50 \mu\text{m} \times 50 \mu\text{m}$. It was noticed for Np1 (Fig. 5b) that the ranges of height of the grains vary from 12 to 82 nm. In this same image were found grains with high density and agglomerates in specific areas of the surface, with a RMS roughness of 9.432 nm. In Fig. 5d, homogeneous grain size was distinguished, and the RMS roughness of Np2 was 136.2 nm. Np2 showed higher grain height (0–0.84 μm); the same behavior was found in the results given by DLS. The information provided by the 2D tapping mode AFM matches with noticeable better definition for the images of Np2 (Fig. 5b) and Np1

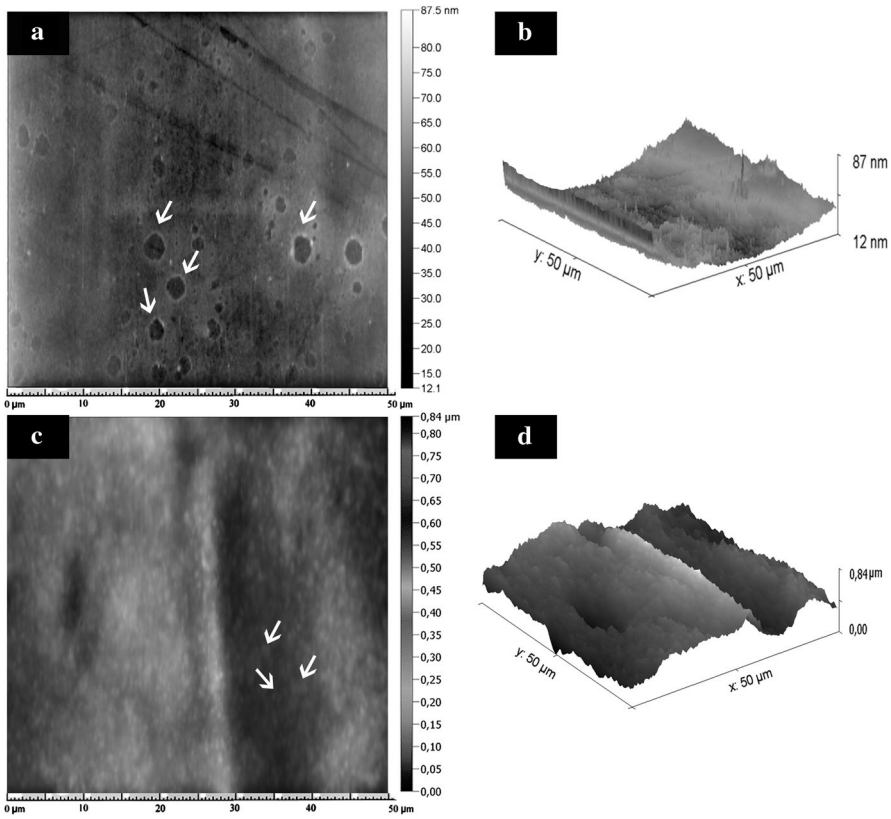


Fig. 5 Two- and three-dimensional view of Np1 (a, b) and Np2 (c, d) showing surface roughness

(Fig. 5a). Np2 presented particles that appeared clearly and seem to be small particles with a size diameter of 1.03 μm. On the other hand, Np1 presented some grains with different sizes, and these are located randomly in the image with an average size of 1.828 μm; this result is due to the agglomerates than increase in the size, and it was related to the higher index of polydispersity compared with Np2.

Morphology, size, composition and specific superficial area

Morphology

In order to define the surface morphology of the cross-linked particles, micrographs at different sizes of 200, 60 and 20 were taken from the samples. In Fig. 6a–c, Np1 presented an agglomerate of particles, which together tends to sphericity. Its lumps were observed, with a crystalline appearance, and edges along the surface layer were found. A porous and no plane surface of the particles was noted; in general, there is a lack of shape, confirming the observations of high density obtained by AFM.

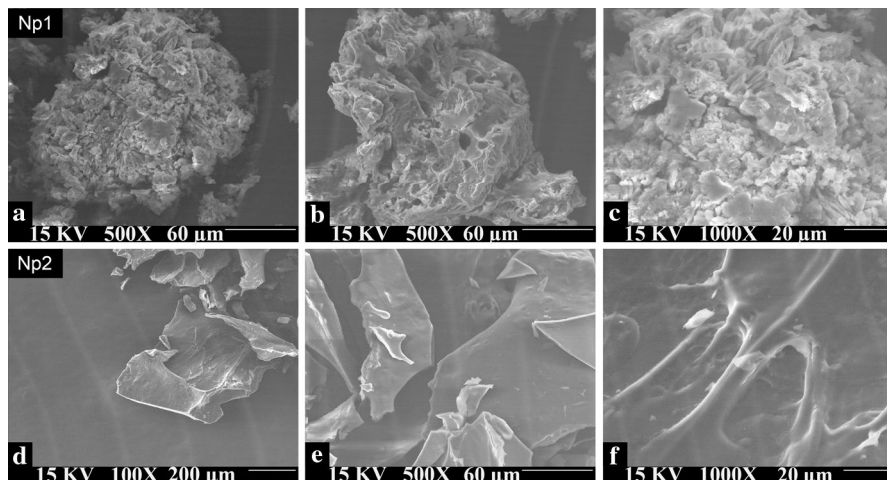


Fig. 6 SEM images of chitosan nanoparticles Np1 (a–c) and Np2 (d–f)

Np2 particles shown in Fig. 6d–f have been recognized to be amorphous, with certain areas of long flat surface. Long and breakable flakes being spliced can be observed, revealing the existence of various material sizes. Although the particles were cross-linked using the same agent, they showed a totally different appearance; hence, it is deduced that the method utilized to synthesize changed the condition of the surface.

Composition and specific superficial area and solubility

The elements present in the nanoparticles were measured using a complementary analysis (EDS). The characteristic elements in chitosan, such as carbon, hydrogen, oxygen and nitrogen, were obtained (Fig. 7). Additionally, phosphorous and sodium were found to be a distinctive element of cross-linked nanoparticles. Np1 presented higher specific superficial area ($1.829 \text{ m}^2/\text{g}$) compared with Np2 ($0.7409 \text{ m}^2/\text{g}$); these results were determined by BET. This fact is related to the morphology found in SEM and attributed to the porous surface, and it is also related to TEM due to the minor size of the particle. A higher specific superficial area was obtained by Shekhawat et al. [26], compared with the area obtained in this study. These findings suggest that nanoparticles with high internal porosity have a relatively high specific superficial area. The low specific superficial area of Np2 is due to the absence of active spaces. This result is related to the findings in SEM. On the other hand, the solubility of Np1 and Np2 is reported to be insoluble in acid media. TPP cross-linking conferred this condition on the nanoparticles by increasing its resistance.

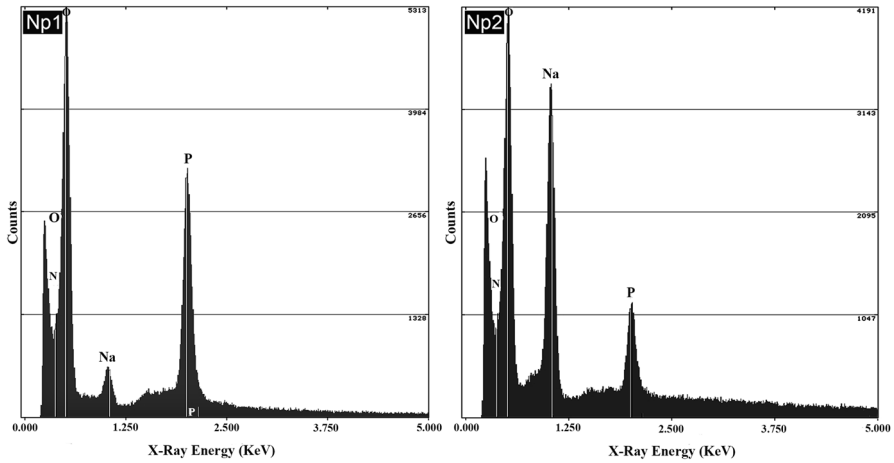


Fig. 7 EDS image of Np1 and Np2

Size

The interaction between the cross-linking agent and chitosan was defined by FTIR and XRD, but the answer to Np1 and Np2 formation was defined by TEM (Fig. 8); then, it was compared with DLS.

In the image of Np1 (Fig. 8a) was appreciated a unimodal distribution recognized as micellar formation, meaning that occur a nucleation in the growing of particles with a circular form. For Np2 (Fig. 8d), it can be visualized as sub-particles of less diameter supported in an array, as well as the literature reported by Ramos Guivar et al. [27]. In both micrographs, particles less than 0.2 μm were noticed.

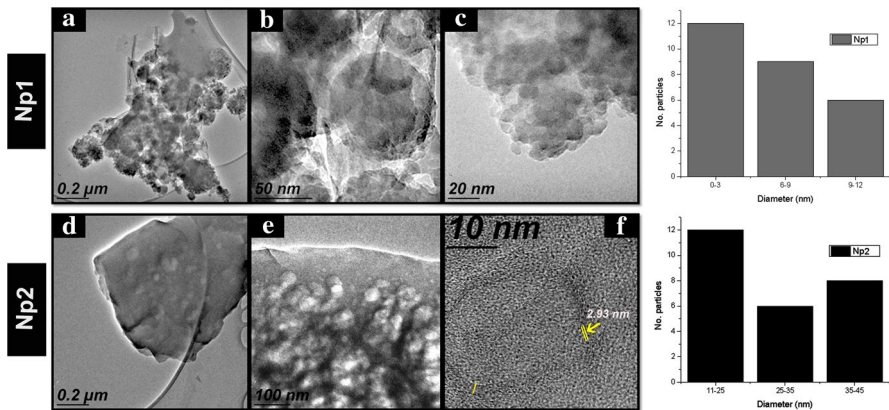


Fig. 8 TEM images of chitosan nanoparticles Np1 (a–c) and Np2 (d–f), and the diameter distribution of Np1 and Np2 histogram

A micrograph at 50 and 100 nm was taken to obtain more details of the size of the nanoparticles, and those are shown in Fig. 8b and e. In both cases, encapsulated particles were observed in an array. Np2 (Fig. 8e) resulted with well-defined circular shape particles with the same condition occurred with Np1 (Fig. 8b) that presented a perfect circular formation with a size of 92.3 nm. Another shot of images at 20 nm was taken for Np1 (Fig. 8c), and the average diameter obtained by TEM was 7.06 nm. The average diameter measurement of Np2 (Fig. 8e) was 27.64 nm. In Fig. 8f, planes were distinguished in the perimeter, resulting with an inter-planar distance of 2.93 nm. TEM confirms that TPP was cross-linked with chitosan, and there exists a change in the crystallinity. The analysis of the diameter distribution (Fig. 8) presented the smallest size for Np1 from 0 to 3 nm, and for Np2 the smallest size was found in a range of 11–25 nm.

Size distributions of Np1 and Np2 were determined by DLS (Fig. 9). The size of the Np1 (Fig. 9a) was in the range of 100–1000 nm, the mean diameter was 315.5 nm and a PDI of 0.353. The mean diameter of Np2 (Fig. 9b) was 437.4 nm with a PDI of 0.273, varying the size from 110 to 1500 nm. The disparity of the size between DLS and TEM of Np1 and Np2 was associated with the solid state of the TEM measurement, while DLS derives the result from an aqueous solution, resulting in a hydrodynamic diameter. Ding et al. [28] acquired a mean diameter of 211.50 ± 1.58 nm by ionic gelation method, coincidentally with a particle size variation from 100 to 1000 nm, comparable with this study.

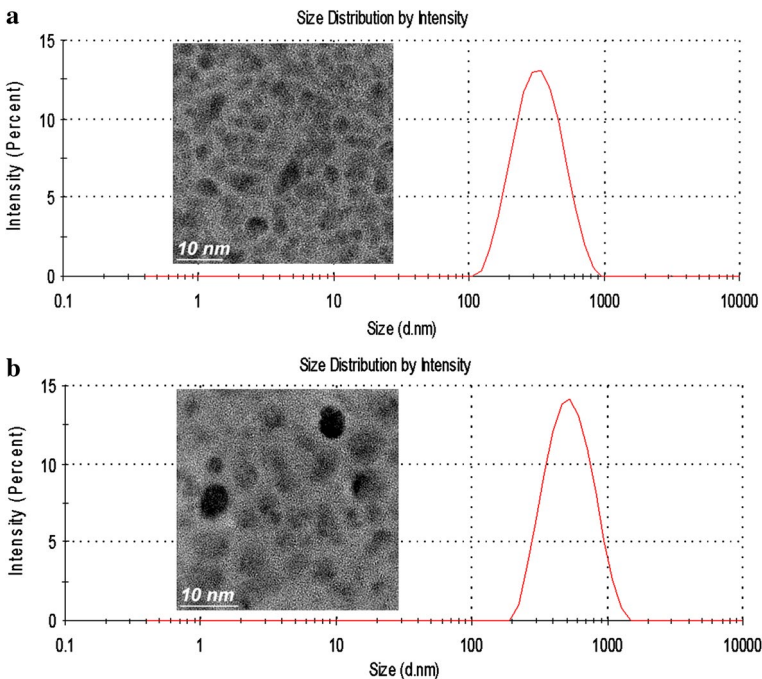


Fig. 9 Size distribution of **a** Np1 and **b** Np2

Following up the two methods, it resulted in a smaller diameter size for Np1 than for Np2. Regarding the TPP doses, is clear that the high concentration for Np1 (Fig. 1) induces to a decrease in the particle size; and this is a result of the arrangement of strong networks between the polymer and the cross-linker, similar data were described by Sheikholeslami et al. [29].

On the other hand, the time stirring at 100 rpm by 36 and 24 h for Np1 and Np2, respectively, did not affect the particle size. The biggest influence is due to TPP concentration. Fan et al. [30] proved that the distribution size was significantly reduced by increasing the stirring speed from 200 to 800 rpm, but also a continuous increase in stirring leads to the aggregation of the particles, because it may destroy the repulsive forces in the ionic gelation process; this is the reason why, in this work, a low stirring speed was used (100 rpm).

According to the preparation method, Np2 was prepared with low TPP dosage and low chitosan concentration with high DA. These three variables mentioned before produce an increment in the particle size compared with Np1 (Fig. 1); in this way, the information reported by Sreekumar et al. [31] affirmed that chitosan concentration and degree of deacetylation play an important role in the formation of micro- and nanoparticles, and these two factors have a strongest influence over size, which was observed in the particle size of Np2.

Allura red adsorption

The results of the evaluation of dye removal expressed in percentage of removal (R%) of Np1 and Np2 are observed in Fig. 10a, b. As shown in Fig. 10a of Np1, dye removal revealed the following order, pH 2 > pH 4 > pH 6, in a range of 59.53–100%. The maximum percentage of dye removal was achieved at pH 2 from 0.01 to 0.05 g. The mechanism of adsorption process of RA dye being in acid solution makes dissociate dye sulfonate groups (SO^{3-}) to transform to anions, and by the presence of hydrogen the free amino groups (NH^{3+}) are protonated allowing the attraction between these opposite ions [32]. Same evaluation was realized to Np2

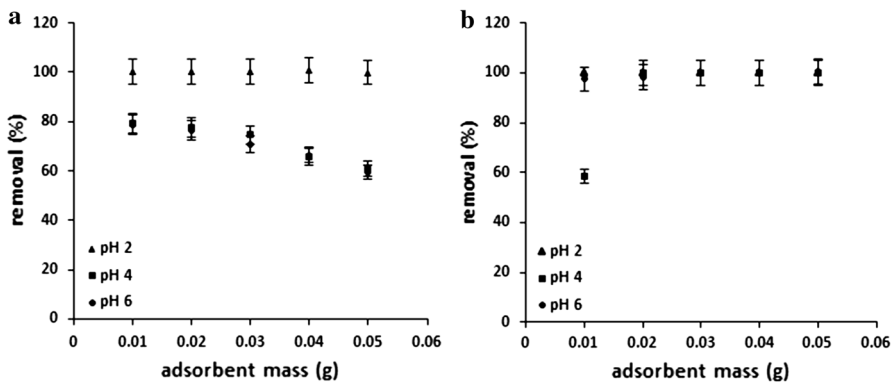


Fig. 10 Effect of mass adsorbent of **a** nanoparticles by ionic gelation method 1 (Np1) and **b** ionic gelation method 2 (Np2) on RA dye removal

and is observed in Fig. 10b, and dye removal in Np2 indicated the highest percentages of removal at all pHs compared to Np1.

The information of Np1 exhibited that an increase in adsorbent mass decreases the percentage of dye removal. A similar phenomenon was reported by Shajahan et al. [33] who concluded that some larger structure dyes are not able to penetrate the internal pore structure of nanoparticle of chitosan because of its size; preferentially dyes adsorb near to the outer surface of the particle, which decreases the adsorption. It is also appreciated in Fig. 10a, b that the optimal adsorbent mass in Np1 and Np2 was 0.01 g at pH 2. Studies investigated by Hosseini et al. [33] by using chitosan–TPP magnetic nanogels revealed a double dosage of mass of adsorbent in comparison with these studies to remove methyl orange dye, under acidic conditions. Harnessing the last information, the effect of contact time was evaluated in Np1 and Np2 at an interval time from 0 to 25 min. Results in Np1 and Np2 indicated an insignificant increase of dye removal when increasing the time, due to the complete dye removal (99.99–100%). Starting from 5 until 25 min, the percentage of dye removal remained constant; under this condition, the optimal contact time was 5 min in Np1 and Np2. Similar results were published by Azlan et al. [34].

Conclusions

Cross-linked nanoparticles were synthesized by two ionic gelation methods in which the variation was the dosage of TPP, and stirring time, chitosan concentration and chitosan deacetylation degree (92.16%) are kept constant. Np1 and Np2 characteristics were studied and compared by FTIR, AFM, XRD, SEM–EDS, TEM, DLS, BET and solubility test, which confirmed that chitosan was cross-linking with TPP to form nanoparticles. Np1 and Np2 resulted with a mean diameter of 315.5 nm and 437.4 nm, respectively, both with low polydispersity (0.273–0.353). The influence on smaller particle size was defined by a low concentration of chitosan solution (0.2 mg/mL) and higher dosage of TPP (1 mg/mL), while the stirring time at 100 rpm by 36 and 24 h for Np1 and Np2, respectively, did not affect in particle size. The allura red dye removal in Np1 and Np2 was studied. The results showed the maximum dye removal percentage in Np1 and Np2 using 0.01 g of mass adsorbent (99.99–100%) at pH 2. Moreover, Np1 exhibited a low removal dye percentage when increasing the adsorbent mass at pH 4 and 6, due to its higher polydispersity compared with Np2 that tends to form agglomerates than to avoid the adsorption even when the superficial area is higher. Although the mean diameter was higher in Np1, Np2 was recognized as the best adsorbent by exhibiting high allura red dye removal percentage under several pHs.

Acknowledgements The authors are grateful for the financial support project PROFAPI_2017_0121 from Instituto Tecnológico de Sonora. The first author is grateful to CONACYT (269728).

Compliance with ethical standards

Conflict of interest The authors declare that they have no conflict of interest.

References

1. Rinaudo M (2006) Chitin and chitosan: properties and applications. *Prog Polym Sci* 31(7):603–632. <https://doi.org/10.1016/j.progpolymsci.2006.06.001>
2. Gazori T, Khoshayand MR, Azizi E, Yazdizade P, Nomani A, Haririan I (2009) Evaluation of Alginate/Chitosan nanoparticles as antisense delivery vector: formulation, optimization and in vitro characterization. *Carbohyd Polym* 77(3):599–606. <https://doi.org/10.1016/j.carbpol.2009.02.019>
3. Banerjee T, Mitra S, Kumar Singh A, Kumar Sharma R, Maitra A (2002) Preparation, characterization and biodistribution of ultrafine chitosan nanoparticles. *Int J Pharm* 243(1–2):93–105. [https://doi.org/10.1016/S0378-5173\(02\)00267-3](https://doi.org/10.1016/S0378-5173(02)00267-3)
4. Höhne S, Frenzel R, Heppe A, Simon F (2007) Hydrophobic chitosan microparticles: heterogeneous phase reaction of chitosan with hydrophobic carbonyl reagents. *Biomacromol* 8(7):2051–2058. <https://doi.org/10.1021/bm0702354>
5. Sacco P, Paoletti S, Cok M, Asaro F, Abrami M, Grassi M, Donati I (2016) Insight into the ionotropic gelation of chitosan using tripolyphosphate and pyrophosphate as cross-linkers. *Int J Biol Macromol* 92:476–483. <https://doi.org/10.1016/j.ijbiomac.2016.07.056>
6. Liu D, Wei Y, Yao P, Jiang L (2006) Determination of the degree of acetylation of chitosan by UV spectrophotometry using dual standards. *Carbohyd Res* 341(6):782–785. <https://doi.org/10.1016/j.carres.2006.01.008>
7. Hashad RA, Ishak RAH, Fahmy S, Mansour S, Geneidi AS (2016) Chitosan-tripolyphosphate nanoparticles: optimization of formulation parameters for improving process yield at a novel pH using artificial neural networks. *Int J Biol Macromol* 86:50–58. <https://doi.org/10.1016/j.ijbiomac.2016.01.042>
8. Moussavi G, Mahmoudi M (2009) Removal of azo and anthraquinone reactive dyes from industrial wastewaters using MgO nanoparticles. *J Hazard Mater* 168(2):806–812. <https://doi.org/10.1016/j.jhazmat.2009.02.097>
9. Lipatova IM, Makarova LI, Yusova AA (2018) Adsorption removal of anionic dyes from aqueous solutions by chitosan nanoparticles deposited on the fibrous carrier. *Chemosphere* 212:1155–1162. <https://doi.org/10.1016/j.chemosphere.2018.08.158>
10. Li C, Lou T, Yan X, Y-z Long, Cui G, Wang X (2017) Fabrication of pure chitosan nanofibrous membranes as effective absorbent for dye removal. *Int J Biol Macromol*. <https://doi.org/10.1016/j.ijbiomac.2017.08.072>
11. El-Harby NF, Ibrahim SMA, Mohamed NA (2017) Adsorption of Congo red dye onto antimicrobial terephthaloyl thiourea cross-linked chitosan hydrogels. *Water Sci Technol* 10:11–12. <https://doi.org/10.2166/wst.2017.442>
12. Calvo PRC, Vila JLL, Alonso MJ (1997) Novel hydrophilic chitosan-polyethylene oxide nanoparticles as protein carriers. *J Appl Polym Sci* 63:125–132
13. Hu ZG, Zhang J, Chan WL, Szeto YS (2006) The sorption of acid dye onto chitosan nanoparticles. *Polymer* 47(16):5838–5842. <https://doi.org/10.1016/j.polymer.2006.05.071>
14. Sini TK, Santhosh S, Mathew PT (2007) Study on the production of chitin and chitosan from shrimp shell by using *Bacillus subtilis* fermentation. *Carbohyd Res* 342(16):2423–2429. <https://doi.org/10.1016/j.carres.2007.06.028>
15. Kong X (2012) Simultaneous determination of degree of deacetylation, degree of substitution and distribution fraction of –COONa in carboxymethyl chitosan by potentiometric titration. *Carbohyd Polym* 88(1):336–341. <https://doi.org/10.1016/j.carbpol.2011.12.019>
16. De Andrade SMB, Ladchumananandasivam R, Da Rocha BG, Belarmino DD, Galvao OA (2012) The use of exoskeletons of shrimp (*Litopenaeus vanammei*) and crab (*Ucides cordatus*) for the extraction of chitosan and production of nanomembrane. *MSA* 3:495–508. <https://doi.org/10.4236/msa.2012.37070>
17. Dimzon IKD, Ebert J, Knepper TP (2013) The interaction of chitosan and olive oil: effects of degree of deacetylation and degree of polymerization. *Carbohyd Polym* 92(1):564–570. <https://doi.org/10.1016/j.carbpol.2012.09.035>
18. Brugnerotto J, Lizardi J, Goycoolea FM, Argüelles-Monal W, Desbrières J, Rinaudo M (2001) An infrared investigation in relation with chitin and chitosan characterization. *Polymer* 42(8):3569–3580. [https://doi.org/10.1016/S0032-3861\(00\)00713-8](https://doi.org/10.1016/S0032-3861(00)00713-8)
19. Macea RB, De Hoyos CF, Montes YG, Fuentes EM, Ruiz JIR (2015) Síntesis y propiedades de filmes basados en quitosano/lactosuero. *Polímeros* 25:58–69. <https://doi.org/10.1590/0104-1428.1558>

20. Lin C-C, Lin C-W (2009) Preparation of N, O-carboxymethyl chitosan nanoparticles as an insulin carrier. *Drug Deliv* 16(8):458–464. <https://doi.org/10.3109/10717540903353090>
21. Sun S, Wang A (2006) Adsorption kinetics of Cu(II) ions using N,O-carboxymethyl-chitosan. *J Hazard Mater* 131(1–3):103–111. <https://doi.org/10.1016/j.jhazmat.2005.09.012>
22. Nosal WH, Thompson DW, Yan L, Sarkar S, Subramanian A, Woollam JA (2005) UV–Vis-infrared optical and AFM study of spin-cast chitosan films. *Colloid Surface B* 43(3–4):131–137. <https://doi.org/10.1016/j.colsurfb.2004.08.022>
23. Martins AF, de Oliveira DM, Pereira AGB, Rubira AF, Muniz EC (2012) Chitosan/TPP microparticles obtained by microemulsion method applied in controlled release of heparin. *Int J Biol Macromol* 51(5):1127–1133. <https://doi.org/10.1016/j.ijbiomac.2012.08.032>
24. Walke S, Srivastava G, Nikalje M, Doshi J, Kumar R, Ravetkar S, Doshi P (2015) Fabrication of chitosan microspheres using vanillin/TPP dual crosslinkers for protein antigens encapsulation. *Carbohydr Polym* 128:188–198. <https://doi.org/10.1016/j.carbpol.2015.04.020>
25. Deshpande P, Dapkekar A, Oak MD, Paknikar KM, Rajwade JM (2017) Zinc complexed chitosan/TPP nanoparticles: a promising micronutrient nanocarrier suited for foliar application. *Carbohydr Polym* 165:394–401. <https://doi.org/10.1016/j.carbpol.2017.02.061>
26. Shekhawat A, Kahu S, Saravanan D, Jugade R (2017) Tin(IV) cross-linked chitosan for the removal of As(III). *Carbohydr Polym* 172:205–212. <https://doi.org/10.1016/j.carbpol.2017.05.038>
27. Ramos Guivar JA, Sanches EA, Bruns F, Sadrollahi E, Morales MA, López EO, Litterst FJ (2016) Vacancy ordered γ -Fe₂O₃ nanoparticles functionalized with nanohydroxyapatite: xRD, FTIR, TEM, XPS and Mössbauer studies. *Appl Surf Sci* 389:721–734. <https://doi.org/10.1016/j.apsusc.2016.07.157>
28. Ding R-L, Xie F, Hu Y, Fu S-Z, Wu J-B, Fan J, He W-F, He Y, Yang L-L, Lin S, Wen Q-L (2017) Preparation of endostatin-loaded chitosan nanoparticles and evaluation of the antitumor effect of such nanoparticles on the Lewis lung cancer model. *Drug Deliv* 24(1):300–308. <https://doi.org/10.1080/10717544.2016.1247927>
29. Sheikholeslami ZS, Salimi-Kenari H, Imani M, Atai M, Nodehi A (2017) Exploring the effect of formulation parameters on the particle size of carboxymethyl chitosan nanoparticles prepared via reverse micellar crosslinking. *J Microencapsul* 34(3):270–279. <https://doi.org/10.1080/02652048.2017.1321047>
30. Fan W, Yan W, Xu Z, Ni H (2012) Formation mechanism of monodisperse, low molecular weight chitosan nanoparticles by ionic gelation technique. *Colloids Surf B* 90:21–27. <https://doi.org/10.1016/j.colsurfb.2011.09.042>
31. Sreekumar S, Goycoolea FM, Moerschbacher BM, Rivera-Rodriguez GR (2018) Parameters influencing the size of chitosan-TPP nano- and microparticles. *Sci Rep* 8(1):4695. <https://doi.org/10.1038/s41598-018-23064-4>
32. Zhou L, Jin J, Liu Z, Liang X, Shang C (2011) Adsorption of acid dyes from aqueous solutions by the ethylenediamine-modified magnetic chitosan nanoparticles. *J Hazard Mater* 185(2):1045–1052. <https://doi.org/10.1016/j.jhazmat.2010.10.012>
33. Shajahan A, Shankar S, Sathiyaseelan A, Narayan KS, Narayanan V, Kaviyarasan V, Ignacimuthu S (2017) Comparative studies of chitosan and its nanoparticles for the adsorption efficiency of various dyes. *Int J Biol Macromol* 104:1449–1458. <https://doi.org/10.1016/j.ijbiomac.2017.05.128>
34. Azlan K, Wan Saime WN, Lai Ken L (2009) Chitosan and chemically modified chitosan beads for acid dyes sorption. *J Environ Sci* 21(3):296–302. [https://doi.org/10.1016/S1001-0742\(08\)62267-6](https://doi.org/10.1016/S1001-0742(08)62267-6)